Layer Structured α-Fe 2 O 3 Nanodisk/Reduced Graphene Oxide Composites as High-Performance Anode Materials for Lithium-Ion Batteries

ARTICLE *in* ACS APPLIED MATERIALS & INTERFACES · APRIL 2013

Impact Factor: 6.72 · DOI: 10.1021/am400670d · Source: PubMed

6 AUTHORS, INCLUDING:

Jin Qu
Beijing University of Chemical Technology
28 PUBLICATIONS **430** CITATIONS
SEE PROFILE

Yu-Guo Guo
Chinese Academy of Sciences
170 PUBLICATIONS **10,865** CITATIONS
SEE PROFILE

Wei-Guo Song
Chinese Academy of Sciences
110 PUBLICATIONS **4,622** CITATIONS
SEE PROFILE

ACS APPLIED MATERIALS & INTERFACES

Research Article

www.acsami.org

Layer Structured α-Fe_2O_3 Nanodisk/Reduced Graphene Oxide Composites as High-Performance Anode Materials for Lithium-Ion Batteries

Jin Qu,[†,‡] Ya-Xia Yin,[†] Yong-Qing Wang,[†,‡] Yang Yan,[†,‡] Yu-Guo Guo,*[,†] and Wei-Guo Song*[,†]

[†]Beijing National Laboratory for Molecular Sciences (BNLMS) & Key Laboratory for Molecular Nanostructures and Nanotechnology, Institute of Chemistry, Chinese Academy of Sciences, Beijing 100190, People's Republic of China

[‡]University of Chinese Academy of Sciences, Beijing 100049, People's Republic of China

Supporting Information

ABSTRACT: A composited anode material with combined layered α-Fe_2O_3 nanodisks and reduced graphene oxide was produced by an in situ hydrothermal method for lithium-ion batteries. As thin as about 5-nm-thickness α-Fe_2O_3 nanosheets, open channels, and face-to-face tight contact with reduced graphene oxide via oxygen bridges made the composite have a good cyclability and rate performance, especially at high charge/discharge rates.

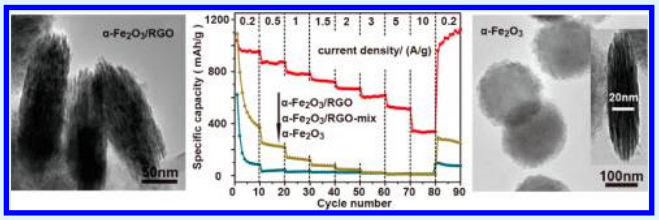

KEYWORDS: *α-Fe_2O_3, layered nanodisk, reduced graphene oxide, oxygen bridges, Li-ion battery*

INTRODUCTION

As the most stable iron oxide under ambient conditions, α-Fe_2O_3 has been extensively used in many fields, such as adsorption[1,2] and catalysis,[3,4] and as sensors[5] and lithium-ion batteries[6−8] because of its low cost and safety and it is environmentally benign. As anode materials for lithium-ion batteries, α-Fe_2O_3 had a higher specific capacity (1007 mAh/g) than conventional graphite (372 mAh/g). However, the repeated conversion reaction caused drastic volume changes (>200%) in each cycle and consequently severe destruction of the electrode upon electrochemical cycles, especially at high rates. Reducing the effective size of the metal oxide particles and constructing open channels in the electrode materials are two main strategies currently employed to improve the cycling and rate properties.[9−12] For example, stacked ultrathin titanate nanosheets with open channels have shown ultrafast lithium storage with an excellent cycle and rate performance.[11] Thus, a rational approach for α-Fe_2O_3 is to build a layered structure that is composed of α-Fe_2O_3 nanosheets. The open spaces between the nanosheets can reduce the impact of volume change. However, poor conductivity is a problem for many metal oxide anode materials.

Because of its excellent electron conductivity, flexibility, chemical stability, and high theoretical surface area (2600 m^2/g), graphene (G) is often integrated with other active materials to improve its electrochemical performance in energy storage devices[13−17] The synergistic effect arising from interactions between G and the active material was crucial because the presence of G could help to sustain the volume change of the active materials and increase their electrical conductivity. For example, the oxygen bridges between G and NiO have been shown to induce a better performance than each individual component and the total sum of the individual effects.[18] Another report showed that the Fe_3O_4/G composite with a tight contact through oxygen bridges had a better lithium-ion storage performance than the Fe_3O_4/G composite with a loose contact.[19] In these composite materials, the contact efficiency of G with the active material was an important factor in influencing the electrochemical performance. Apparently, maximum contact efficiency could be achieved via a face-to-face contact between the G sheet and the active material sheet. Zhi et al. reported that the G-confined tin nanosheets with a face-to-face contact had exhibited a higher lithium storage capacity than that of spherical tin particles being dispersed in the G matrix with a point-to-point contact.[20] Thereby we envisioned that the composite based on layered α-Fe_2O_3 nanodisks and reduced graphene oxide (RGO) might take advantage of all of the above-mentioned structural features for an enhanced lithium-ion storage performance if the Fe−O−C bond was constructed between layered α-Fe_2O_3 and RGO.

In this paper, we fabricated a layered α-Fe_2O_3 nanodisk/reduced graphene oxide (α-Fe_2O_3/RGO) composite through a silicate-anion-assisted in situ hydrothermal method. The oxygen bridges were constructed in a face-to-face manner between ultrathin α-Fe_2O_3 nanosheets and RGO. This face-to-face stacked structure provided a larger effective interaction area between electrode materials and electrolytes, shortened the lithium-ion diffusion path, and improved the kinetics of charge transportation. The layered α-Fe_2O_3/RGO composite displayed excellent lithium storage properties with high specific capacity

Received: February 21, 2013
Accepted: April 2, 2013
Published: April 2, 2013

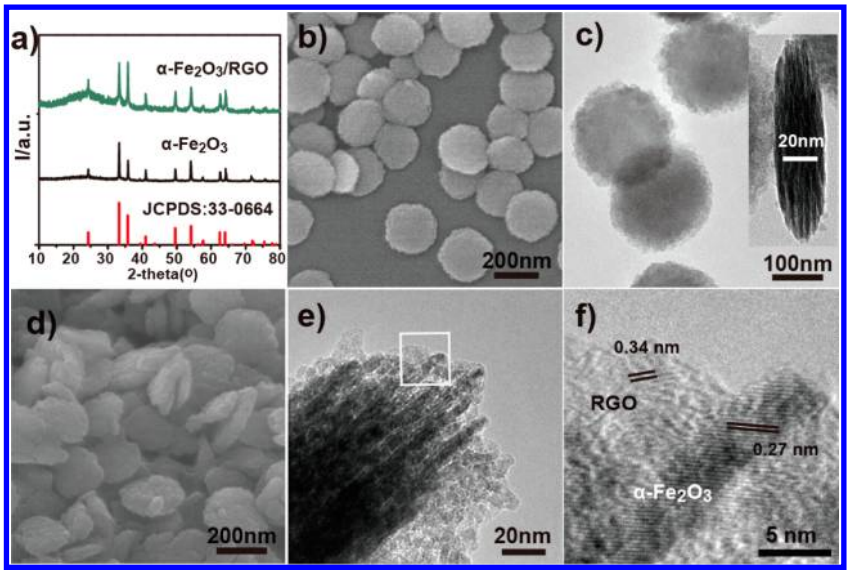

Figure 1. (a) XRD pattern of the as-prepared α-Fe_2O_3/RGO and α-Fe_2O_3. (b) SEM and (c) TEM images of pure α-Fe_2O_3 (inset: side view). (d) SEM and (e) HRTEM images of α-Fe_2O_3/RGO. (f) HRTEM image of the white square in part e.

and stable charge/discharge cyclability (931 mA·h/g after 50 cycles). Even at very high current density (up to 10 A/g), the composite still retains a capacity of 337 mA·h/g.

EXPERIMENTAL SECTION

Materials. Analytical-grade iron chloride, sodium silicate, NaOH, H_2O_2 (3 and 30 wt %), graphite, sulfuric acid, sodium nitrate, $KMnO_4$, and HCl (10 wt %) were purchased from Beijing Chemicals Co. (Beijing, China). All of the chemicals were used as received.

Synthesis of Layered α-Fe_2O_3/RGO, α-Fe_2O_3, and RGO. Graphene oxide (GO) was produced according to the literature.[21] In a typical procedure for the composite, analytical-grade iron chloride (0.75 mmol) and 5 mL of a GO (6 mg/mL) solution were mixed in 25 mL of deionized water as solution A, and sodium silicate (0.375 mmol) was homogeneously dispersed into 20 mL of deionized water as solution B. The above two solutions were then mixed and transferred into an autoclave (70 mL) for 24 h at 140 °C. The brown product was collected by centrifugation and rinsed with distilled water several times. Finally, the product was dried in an oven at 80 °C overnight. α-Fe_2O_3/RGO composites were obtained by treating at 300 °C under argon protection for 2 h. GO alone was also treated under the same conditions to obtain RGO. The α-Fe_2O_3-controlled sample was fabricated without RGO.

Characterization. The microscopic features of the samples were characterized by scanning electron microscopy (SEM; JEOL-6701F), transmission electron microscopy (TEM; JEOL JEM-1011, 100 kV), and high-resolution TEM (HRTEM; JEM 2100F, 200 kV). Powder X-ray diffraction (XRD) patterns were collected on an X-ray diffractometer (Rigaku D/max-2500 diffractometer with Cu Ka radiation, λ = 1.54056 Å) at 40 kV and 200 mA. The surface area of the products was measured by the Brunauer–Emmet–Teller (BET) method using N_2 adsorption and desorption isotherms on an Autosorb-1 analyzer at 78.3 K. For XPS analysis, a Kratos AXIS 165 multitechnique electron spectrometer was used. The micro-Raman analysis (DXR Raman Microscope, Thermo) was used to characterize the samples. Thermogravimetric analysis (TGA) measurements were carried out in an air atmosphere at a heating rate of 10 °C/min using a Perkin-Elmer Diamond TG/DTA instrument.

Electrochemical Measurements. Electrochemical tests were performed using coin-type cells assembled in an argon-filled glovebox. The working electrode was composed of 70 wt % active material (α-Fe_2O_3/RGO, α-Fe_2O_3, or α-Fe_2O_3/RGO-mix), 20 wt % super-P, and 10 wt % poly(vinylidene fluoride) was fabricated by casting a slurry onto a copper foil (99.6%, Goodfellow). The electrolyte was 1 M $LiPF_6$ dissolved in a mixture of ethylene carbonate, dimethyl carbonate, and diethyl carbonate with a weight ratio of 1:1:1 (Tianjin Jinniu Power Sources Material Co., Ltd.). Lithium foil was used as the counterelectrode. A glass fiber (GF/D) from Whatman was used as the separator. Galvanostatic cycling of the assembled cells was carried out using an Arbin BT2000 system in the voltage range of 0.005–3 V (vs Li^+/Li) under a discharge/charge current density of 0.2–10 A/g.

RESULTS AND DISCUSSION

The products' XRD patterns are shown in Figure 1a. All of these sharp peaks could be clearly indexed to α-Fe_2O_3 (JCPDS no. 33-0664). No other impurities were observed. The morphologies were studied by SEM and TEM. α-Fe_2O_3 showed a smooth disklike structure with a diameter of around 200 nm (Figure 1b). The TEM image also showed a disklike morphology constructed with a dozen nanosheets and the layered structure (Figure 1c and inset). The SEM image of α-Fe_2O_3/RGO showed a disk similar to that of α-Fe_2O_3. However, the disks were stuck together (Figure 1d) and are quite different from those of Figure 1b for pure α-Fe_2O_3. No RGO could be observed from the SEM image. The specific surface area (calculated by the Brunauer–Emmett–Teller method, as shown in Figure S1 in the Supporting Information, SI) of the composite increased from 40.6 m^2/g (for a pure α-Fe_2O_3 nanodisk) to 296.7 m^2/g (for an α-Fe_2O_3/RGO composite). Further investigation showed that the surface of the composited disks turned rough compared to pure α-Fe_2O_3 (Figure 1d,e). The HRTEM image in Figure 1e showed that the edge of the layered structure became fuzzy, while the TEM image of pure α-Fe_2O_3 was quite clean (Figure 1c). There might be some nanometer-sized particles anchored on the surface, but the layered structure is still retained (Figure S2 in the SI). Elemental mapping analysis showed that iron, carbon, and oxygen elements were uniformly distributed in the composite structure (Figure S3 in the SI). However, it is really difficult to distinguish RGO and α-Fe_2O_3. RGO might not only wrap α-Fe_2O_3 but also be sandwiched between α-Fe_2O_3 nanosheets. They anchored tightly with each other, and only RGO's edge could be observed in the HRTEM image. As shown in Figure 1f, the composite showed lattice fringes of both RGO and α-Fe_2O_3, confirming that the roughness was

caused by RGO being tightly wrapped around the α-Fe_2O_3 nanosheets. Such tight wrapping resulted in a face-to-face stacked structure between RGO and α-Fe_2O_3 and might be more beneficial to lithium storage than the point-to-point contact mode.[20]

The G bond corresponded to the first-order scattering of the E_{2g} mode observed for sp^2 carbon domains. Also, the chemical link could modify strongly the geometric and electronic structures of G because of the change of hybridization of the carbon atoms. It has been reported that charge transfer between carbon materials and nanomaterials could induce the shift of the G peak of the Raman spectra of the carbon materials, making the location of the G peak in Raman spectra of carbon-based composites an ideal probe to study the interaction between nanomaterials and G.[18,19,22,23] In this study, an 11 cm^{-1} blue shift of the G band was observed. Compared with RGO's G peak located at 1592 cm^{-1}, the G peak of α-Fe_2O_3/RGO shifted to 1603 cm^{-1} (Figure 2a), indicating charge

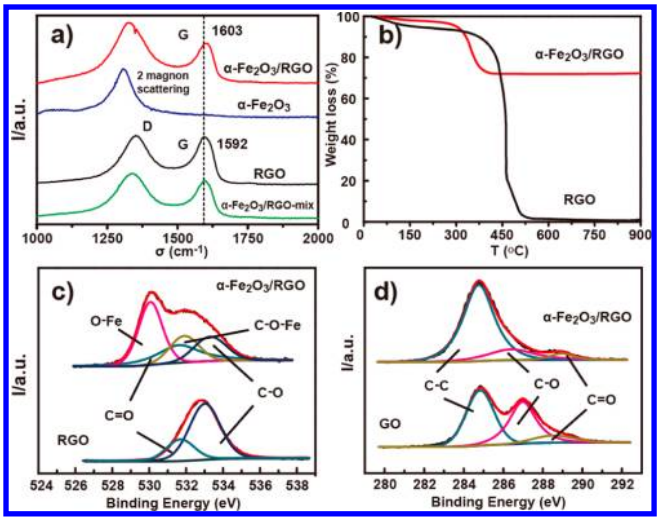

Figure 2. (a) Raman spectra of α-Fe_2O_3/RGO, α-Fe_2O_3, α-Fe_2O_3/RGO-mix, and RGO. (b) TGA and (c) O 1s of α-Fe_2O_3/RGO and RGO. (d) C 1s of α-Fe_2O_3/RGO and GO.

transfer between them. However, no such shift was observed in the physical mixture of α-Fe_2O_3 and RGO. The bands at 1312 cm^{-1} can be ascribed to magnon scattering. Also, the RGO's D peak overlapped with α-Fe_2O_3's magnon scattering peak, so it was not suitable to investigate the shift. α-Fe_2O_3 could also promote the oxidation of carbon through tightly anchored carbon materials but perform hardly any activity in a loose contact.[24−26] TGA analysis showed that the oxidation temperature for α-Fe_2O_3/RGO decreased to around 270 °C, while RGO started to burn at 360 °C (Figure 2b). Such a large decreased temperature indicated that there was tight contact between α-Fe_2O_3 and RGO. XPS spectra of O 1s also supported the conclusion. As shown in Figure 2c, a new peak at 531.9 eV attributed to the Fe−O−C bond was detected in the α-Fe_2O_3/RGO sample. All of this information lead to the conclusion that an effective tight contact was formed. Several studies have shown that such oxygen bridges between metal oxides and G were beneficial to lithium-ion storage.[18,19] The Fe atoms on the oxygenated G might facilitate fast electron hopping from G to α-Fe_2O_3 as well as reversible lithiation/delithiation of α-Fe_2O_3. The C 1s of the sample showed that GO was effectively reduced into RGO (Figure 2d). As reported, RGO would serve as an elastic conductive network for the composite material.[13−17]

The α-Fe_2O_3/RGO composite was used anode materials for lithium-ion batteries, and discharge−charge cycling was carried out in the voltage window of 0.005−3 V (vs Li^+/Li) at 0.2 A/g and ambient temperature. As expected, the α-Fe_2O_3/RGO composite nanomaterials showed a high capacity and a highly stable cyclability. After 50 cycles, the charge capacity remained at 931 mA·h/g compared with the initial charge capacity of 1088 mA·h/g. The compared cycling performances of α-Fe_2O_3 and the α-Fe_2O_3/RGO-mix were also tested under the same conditions. As shown in Figure 3a, owing to α-Fe_2O_3's poor conductivity and much lower BET surface area, the lithium ions and electrons were difficult to transfer to its surface. So, it showed a much lower initial charge capacity than others and then sharply decreased to ~200 mA·h/g within 5 cycles. When RGO was physically mixed with α-Fe_2O_3 with the same ratio as the composite (24.4 wt % RGO determined by TGA analysis; Figure 2b), the lithium storage property was improved compared with α-Fe_2O_3 alone. After 50 cycles, the mixture had a capacity of 244 mA·h/g, while α-Fe_2O_3 had only 89 mA·h/g. However, the mixture's capacity and cyclability was significantly lower than the α-Fe_2O_3/RGO composite. As shown in Figure 3b, the composite had the highest capacity with a 5 mL GO solution during the preparation, indicating that the RGO content could affect the synergistic efficiency between α-Fe_2O_3 and G. Similar content-dependent phenomena were also observed in other carbon-based composite anode materials for lithium-ion batteries.[27−29]

The composite also exhibited a much improved rate performance. Figure 3c showed that the composite remained at 781, 667, and 512 mA·h/g at rates of 1, 2, and 5 A/g after 10 cycles, respectively. When tested at 10 A/g, a decent capacity of 337 mA·h/g was observed on the α-Fe_2O_3/RGO composite, while there was nearly no capacity observed for α-Fe_2O_3 alone and the α-Fe_2O_3/RGO mixture. As shown in Figure 3d, the α-Fe_2O_3/RGO composite had 834, 516, and 261 mA·h/g at 1, 3, and 10 A/g, respectively, after 150 cycles. A slight increase before 70 cycles at the relatively low current density of 1A/g was observed. It might be attributed to improvement of the lithium-ion accessibility in the hybrid during the cycling processes, which led to an increased accommodation behavior for lithium.[30,31] The properties of the α-Fe_2O_3/RGO composite were overall substantially better than those of the α-Fe_2O_3 anode materials in recent reports.[6,31−35]

These excellent properties were credited to the structure of the α-Fe_2O_3/RGO composite, especially the tight contact between α-Fe_2O_3 and RGO. The discharge/charge profiles in the first cycle of the α-Fe_2O_3/RGO, α-Fe_2O_3, and α-Fe_2O_3/RGO-mix samples confirmed the conclusion. Both the α-Fe_2O_3/RGO composite sample and the physical mixed sample had much lower overpotential than α-Fe_2O_3 alone (Figure 4a). However, fast electron hopping from G to α-Fe_2O_3 due to the oxygen bridges allows the α-Fe_2O_3/RGO composite to have the lowest overpotential than the other two samples. Their Nyquist plots (Figure 4b) showed that the diameter of the semicircle for the α-Fe_2O_3/RGO electrode in the high-to-medium-frequency region was much smaller than those of other electrodes, suggesting that the α-Fe_2O_3/RGO electrode possessed much lower contact and charge-transfer resistances. Such a conclusion agreed well with the Raman, XPS, and TGA results that a tight contact between α-Fe_2O_3 and RGO could effectively reduce the contact resistance and enhance charge transfer. The face-to-face

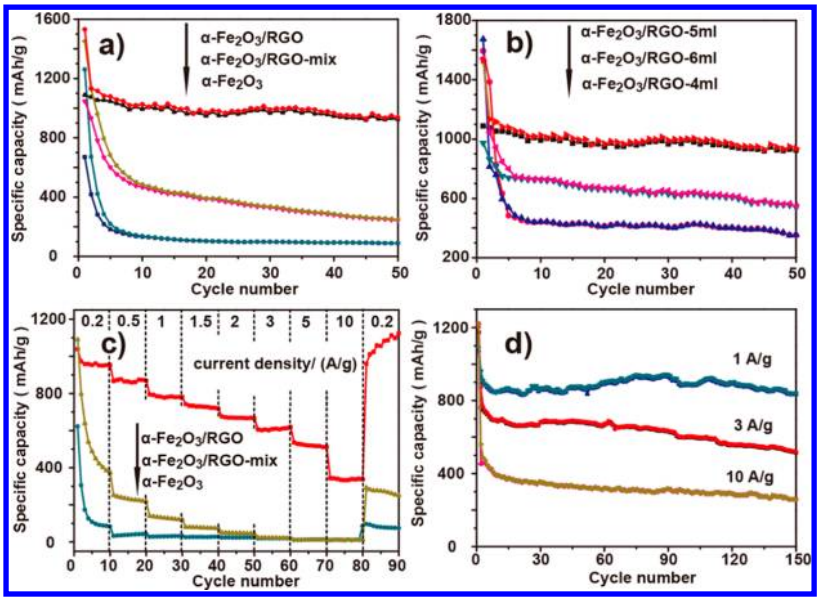

Figure 3. (a) Cycling performance of the electrodes made with α-Fe_2O_3/RGO, α-Fe_2O_3, and α-Fe_2O_3/RGO-mix at a current density of 0.2 A/g within a voltage window of 0.005−3.0 V. (b) Compared cycling performances of the composites with different contents of RGO at a current density of 0.2 A/g within a voltage window of 0.005−3.0 V. (c) Reversible charge capacities of the electrodes cycled at various rates. (d) Long cycling test of the electrodes with α-Fe_2O_3/RGO at 1, 3, and 10 A/g over 150 cycles.

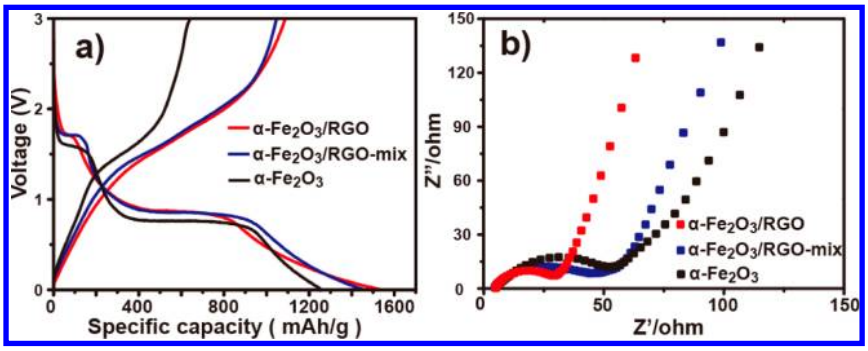

Figure 4. (a) Discharge/charge profiles of α-Fe_2O_3/RGO, α-Fe_2O_3, and α-Fe_2O_3/RGO-mix for the first cycle at a current density of 0.2 A/g. (b) Electrochemical impedance plots of three samples.

wrapping form between α-Fe_2O_3 and RGO offered maximum contact efficiency. As a result, lithium-ion diffusion and electron transfer were expedited at high rates for the composite.

CONCLUSIONS

In summary, we fabricated an α-Fe_2O_3/RGO composite in situ to produce layered α-Fe_2O_3 nanodisks wrapped by RGO sheets around the nanodisks. The oxygen bridges between RGO and α-Fe_2O_3 nanodisks resulted in a synergistic effect to improve the lithium-ion storage behavior of the composite. The excellent electrical conductivity of G, the large contact area between RGO and α-Fe_2O_3, and the layered nanostructure with a short diffusion pathway for lithium ions enhanced the reaction kinetics of the composite. The layered α-Fe_2O_3/RGO composite showed an excellent specific capacity up to 931 mA·h/g after 50 cycles. Even at fast charge/discharge rates of 10 A/g, the composite showed much higher capacity (337 mA·h/g) than the α-Fe_2O_3 nanodisks alone (10 mA·h/g) or the α-Fe_2O_3/RGO-mix (11 mA·h/g).

ASSOCIATED CONTENT

Supporting Information

N_2 adsorption−desorption isotherms of the α-Fe_2O_3 nanodisks and layered α-Fe_2O_3/RGO composite and a HRTEM image and elemental mapping analysis of the side view of the layered α-Fe_2O_3/RGO composite. This material is available free of charge via the Internet at http://pubs.acs.org.

AUTHOR INFORMATION

Corresponding Author

*E-mail: ygguo@iccas.ac.cn (Y.-G.G.), wsong@iccas.ac.cn (W.-G.S.). Tel and Fax: +86-10-62557908 (W.-G.S.).

Notes

The authors declare no competing financial interest.

ACKNOWLEDGMENTS

We gratefully thank the National Basic Research Program of China (Grants 2009CB930400 and 2012CB932900), National Natural Science Foundation of China (Grants NSFC 21121063 and 51225204), and Chinese Academy of Sciences (Grant KJCX2-YW-N41) for financial support.

REFERENCES

(1) Zhong, L. S.; Hu, J. S.; Liang, H. P.; Cao, A. M.; Song, W. G.; Wan, L. J. *Adv. Mater.* **2006**, *18*, 2426−2431.
(2) Cao, C.-Y.; Qu, J.; Yan, W.-S.; Zhu, J.-F.; Wu, Z.-Y.; Song, W.-G. *Langmuir* **2012**, *28*, 4573−4579.
(3) Singh, P. P.; Gudup, S.; Ambala, S.; Singh, U.; Dadhwal, S.; Singh, B.; Sawant, S. D.; Vishwakarma, R. A. *Chem. Commun.* **2011**, *47*, 5852−5854.
(4) Cha, H. G.; Kim, S. J.; Lee, K. J.; Jung, M. H.; Kang, Y. S. *J. Phys. Chem. C* **2011**, *115*, 19129−19135.
(5) Dou, Z.-F.; Cao, C.-Y.; Wang, Q.; Qu, J.; Yu, Y.; Song, W.-G. *ACS Appl. Mater. Interfaces* **2012**, *4*, 5698−5703.
(6) Lin, Y.-M.; Abel, P. R.; Heller, A.; Mullins, C. B. *J. Phys. Chem. Lett.* **2011**, 2885−2891.
(7) Sun, B.; Horvat, J.; Kim, H. S.; Kim, W.-S.; Ahn, J.; Wang, G. *J. Phys. Chem. C* **2010**, *114*, 18753−18761.
(8) Xu, X.; Cao, R.; Jeong, S.; Cho, J. *Nano Lett.* **2012**, *12*, 4988−4991.
(9) Bruce, P. G.; Scrosati, B.; Tarascon, J.-M. *Angew. Chem., Int. Ed.* **2008**, *47*, 2930−2946.
(10) Arico, A. S.; Bruce, P.; Scrosati, B.; Tarascon, J.-M.; van Schalkwijk, W. *Nat. Mater.* **2005**, *4*, 366−377.
(11) Liu, J.; Chen, J. S.; Wei, X.; Lou, X. W.; Liu, X.-W. *Adv. Mater.* **2011**, *23*, 998−1002.
(12) Poizot, P.; Laruelle, S.; Grugeon, S.; Dupont, L.; Tarascon, J. M. *Nature* **2000**, *407*, 496−499.
(13) Xin, S.; Guo, Y.-G.; Wan, L.-J. *Acc. Chem. Res.* **2012**, *45*, 1759−1769.
(14) Xue, D.-J.; Xin, S.; Yan, Y.; Jiang, K.-C.; Yin, Y.-X.; Guo, Y.-G.; Wan, L.-J. *J. Am. Chem. Soc.* **2012**, *134*, 2512−2515.
(15) Jiang, K.-C.; Xin, S.; Lee, J.-S.; Kim, J.; Xiao, X.-L.; Guo, Y.-G. *Phys. Chem. Chem. Phys.* **2012**, *14*, 2934−2939.
(16) Zhou, X.; Yin, Y.-X.; Wan, L.-J.; Guo, Y.-G. *Adv. Energy Mater.* **2012**, *2*, 1086−1090.
(17) Hwang, H.; Kim, H.; Cho, J. *Nano Lett.* **2011**, *11*, 4826−4830.
(18) Zhou, G.; Wang, D.-W.; Yin, L.-C.; Li, N.; Li, F.; Cheng, H.-M. *ACS Nano* **2012**, *6*, 3214−3223.
(19) Zhou, J.; Song, H.; Ma, L.; Chen, X. *RSC Adv.* **2011**, *1*, 782−791.
(20) Luo, B.; Wang, B.; Li, X.; Jia, Y.; Liang, M.; Zhi, L. *Adv. Mater.* **2012**, *24*, 3538−3543.
(21) Zhang, L.-S.; Jiang, L.-Y.; Yan, H.-J.; Wang, W. D.; Wang, W.; Song, W.-G.; Guo, Y.-G.; Wan, L.-J. *J. Mater. Chem.* **2010**, *20*, 5462−5467.
(22) Niyogi, S.; Bekyarova, E.; Itkis, M. E.; Zhang, H.; Shepperd, K.; Hicks, J.; Sprinkle, M.; Berger, C.; Lau, C. N.; deHeer, W. A.; Conrad, E. H.; Haddon, R. C. *Nano Lett.* **2010**, *10*, 4061−4066.
(23) Dresselhaus, M. S.; Jorio, A.; Hofmann, M.; Dresselhaus, G.; Saito, R. *Nano Lett.* **2010**, *10*, 751−758.
(24) Neeft, J. P. A.; van Pruissen, O. P.; Makkee, M.; Moulijn, J. A. *Appl. Catal., B* **1997**, *12*, 21−31.
(25) Neeft, J. P. A.; Makkee, M.; Moulijn, J. A. *Chem. Eng. J.* **1996**, *64*, 295−302.
(26) Neri, G.; Bonaccorsi, L.; Donato, A.; Milone, C.; Musolino, M. G.; Visco, A. M. *Appl. Catal., B* **1997**, *11*, 217−231.
(27) Yue, W.; Lin, Z.; Jiang, S.; Yang, X. *J. Mater. Chem.* **2012**, *22*, 16318−16323.
(28) Ban, C.; Wu, Z.; Gillaspie, D. T.; Chen, L.; Yan, Y.; Blackburn, J. L.; Dillon, A. C. *Adv. Mater.* **2010**, *22*, E145−E149.
(29) Chang, K.; Chen, W.; Ma, L.; Li, H.; Li, H.; Huang, F.; Xu, Z.; Zhang, Q.; Lee, J.-Y. *J. Mater. Chem.* **2011**, *21*, 6251−6257.
(30) Zhou, X.; Wan, L.-J.; Guo, Y.-G. *Adv. Mater.* **2013**, DOI: 10.1002/adma.201300071 (access date: March 29, 2013).
(31) Wang, Z.; Luan, D.; Madhavi, S.; Hu, Y.; Lou, X. W. *Energy Environ. Sci.* **2012**, *5*, 5252−5256.
(32) Zhu, X.; Zhu, Y.; Murali, S.; Stoller, M. D.; Ruoff, R. S. *ACS Nano* **2011**, *5*, 3333−3338.
(33) Reddy, M. V.; Yu, T.; Sow, C. H.; Shen, Z. X.; Lim, C. T.; Subba Rao, G. V.; Chowdari, B. V. R. *Adv. Funct. Mater.* **2007**, *17*, 2792−2799.
(34) Wang, B.; Chen, J. S.; Wu, H. B.; Wang, Z.; Lou, X. W. *J. Am. Chem. Soc.* **2011**, *133*, 17146−17148.
(35) Zhu, J.; Yin, Z.; Yang, D.; Sun, T.; Yu, H.; Hoster, H. E.; Hng, H. H.; Zhang, H.; Yan, Q. *Energy Environ. Sci.* **2013**, *6*, 987−993.